Nanotechnology

Broadband photodetector based on SnTe nanofilm/n-Ge heterostructure

To cite this article before publication: Liyuan Song *et al* 2022 *Nanotechnology* in press https://doi.org/10.1088/1361-6528/ac80cc

IOP Publishing Journal Title
Journal **XX** (XXXX) XXXXXX https://doi.org/XXXX/XXXX

Broadband photodetector based on SnTe nanofilm/n-Ge heterostructure

Liyuan Song[1, 2, 3], Libin Tang[1, 2, 3, *], Qun Hao[1,*], Kar Seng Teng[4,*], Hao Lv[2], Jingyu Wang[2], Jiangmin Feng[2], Yan Zhou[2], Wenjin He[2], Wei Wang[2]

[1] The Laboratory of Photonics Information Technology, Ministry of Industry and Information Technology, School of Optics and Photonics, Beijing Institute of Technology, Beijing 100081, People's Republic of China
[2] Kunming Institute of Physics, Kunming 650223, People's Republic of China
[3] Yunnan Key Laboratory of Advanced Photoelectronic Materials & Devices, Kunming 650223, People's Republic of China
[4] Department of Electronic and Electrical Engineering, Swansea University, Bay Campus, Fabian Way, Swansea SA1 8EN, United Kingdom

E-mail: scitang@163.com (L. B. Tang), qhao@bit.edu.cn (Q. Hao) and k.s.teng@swansea.ac.uk (K. S. Teng)

Received xxxxxx
Accepted for publication xxxxxx
Published xxxxxx

Abstract

Combining novel two-dimensional (2D) materials with traditional semiconductors to form heterostructures for photoelectric detection have attracted great attention due to their excellent photoelectric properties. In this study, we reported the formation of a heterostructure comprising of tin telluride (SnTe) and germanium (Ge) by a simple and efficient one-step magnetron sputtering technique. A photodetector was fabricated by sputtering a nanofilm of SnTe on to a pre-masked n-Ge substrate. *J-V* measurements obtained from the SnTe/n-Ge photodetector demonstrated diode and photovoltaic characteristics in the visible to near-infrared band (*i.e.*, 400-2050 nm). Under near-infrared illumination at 850 nm with an optical power density of 13.81 mW/cm^2, the SnTe/n-Ge photodetector exhibited a small open-circuit voltage of 0.05 V. It also attained a high responsivity (R) and detectivity (D^*) of 617.34 mA/W (at bias voltage of -0.5 V) and 2.33×10^{11} cmHz$^{1/2}$W^{-1} (at zero bias), respectively. Therefore, SnTe nanofilm/n-Ge heterostructure is highly suitable for used as low-power broadband photodetector due to its excellent performances and simple device configuration.

Keywords: SnTe/n-Ge heterostructure, photodetector

1. Introduction

Photodetector based on heterostructure materials is of great interest in the field of photoelectric detection because of its built-in electric field, which can improve the separation and transmission efficiency of photocarriers, hence enhancing the photodetection performance of the device. In recent years, the use of 2D materials in the formation of heterostructures for photoelectric detection have attracted much attention due to its many advantages, such as high electron mobility at room temperature, adjustable band structure with thickness and strain (to achieve adjustable photoelectric performance), excellent mechanical properties (to prepare flexible devices) and so on. For example, 2D tin telluride (SnTe) has many unique properties, such as gapless topological surface states, narrow band gap [1, 2] and high hole mobility [3, 4] at room temperature, and is considered the first topological crystal insulator (TCI) as predicted

theoretically [5] and verified experimentally [6]. SnTe has the potential for use in the development of novel photodetectors with broad spectrum and ultra-fast response requiring minimal energy consumption. However, SnTe is rarely studied for application in photoelectric detection.

Several SnTe photoconductive detectors have been reported in recent years. For example, SnTe/Bi_2Te_3/$SrTiO_3$ photoconductive detector [7] was prepared by molecular beam epitaxy (MBE). The Bi_2Te_3 buffer layer was used to minimize the effect of lattice mismatch between $SrTiO_3$ substrate and SnTe film. The photodetector exhibited stable photoelectric responses in the range of 405-3800 nm, which suggested the potential use of SnTe material in broadband photoelectric detection. Flexible photoconductive detector was produced by depositing SnTe nanoplates on to mica by chemical vapor deposition (CVD) [8]. Under 980 nm laser irradiation, the measured R and D^* were 698 mA/W and 3.89×10^8 $cmHz^{1/2}W^{-1}$ at a bias of 0.5 V, respectively. This demonstrated the application of SnTe nanoplates in the near-infrared (NIR) detection. More recently, SnTe quantum dots/Si photoconductive detector was prepared by spin-coating [9]. The device exhibited a photoelectric response at 2 μm, however it revealed a relatively low R and D^* of 0.03 mA/W and 1.4×10^6 $cmHz^{1/2}W^{-1}$ at 10 V bias voltage, respectively. Therefore, it is of interest to study SnTe based photovoltaic detector to improve the performance of the detector. The fabrication of the heterostructure of SnTe and other n-type semiconductors is expected to be an effective way to greatly improve the separation and transport of photogenerated carriers in SnTe. Moreover, it is easier to prepare low power and large array focal plane array (FPA) detectors by using photovoltaic structure.

So far, only silicon and Bi_2Se_3 have been reported as n-type substrates in the preparation of SnTe based photo detectors. For example, SnTe/n-Si heterostructure [10] prepared using CVD demonstrated photoelectric response (at negative bias) under 808 nm laser irradiation (6.4 $\mu W/cm^{-2}$) with relatively good R and D^* of 128 mA/W and 8.4×10^{12} $cmHz^{1/2}W^{-1}$, respectively. The strong response of SnTe/Si heterostructure to near-infrared (NIR) light is desirable for the development of low-cost and high-performance NIR detectors in the communication band. Photodetector consisting of SnTe/Bi_2Se_3 heterostructure was prepared by a two-step physical vapor deposition (PVD) technique [11]. The device exhibited R and D^* of 145.74 mA/W and 1.15×10^{10} $cmHz^{1/2}W^{-1}$, respectively, in the NIR band of 1550 nm and has potential application in low power consumption and low-cost photoelectric detection. Although the above performance parameters of the SnTe based photovoltaic detectors are favorable, there is still room for improvement. The use of a suitable alternative substrate may improve the performance of SnTe based photodetectors. Also, the use of a low-cost preparation method for the heterostructure is important to ensure commercial viability of the device.

Herein, we reported for the first time on the use of n-Ge, which is a traditional semiconducting material, as a substrate to form heterostructure with SnTe nanofilm. The vertical heterostructure of SnTe/n-Ge was prepared on a pre-masked n-Ge substrate by a simple and efficient method using a one-step RF magnetron sputtering. The sputtered SnTe nanofilm was crystallized without increasing the substrate temperature and with no post-annealing treatment. The SnTe/n-Ge photodetector showed a significant diode rectification characteristic at a small bias range between -0.5 V and 0.5 V, which indicated photovoltaic effect. The photodetector demonstrated photoelectric response over a broadband range from 400 to 2050 nm and exhibited higher responsivity (R) of 617.34 mA/W and detectivity (D^*) of 2.33×10^{11} $cmHz^{1/2}W^{-1}$ in the NIR band of 850 nm at 300 K. Hence, the novel SnTe/n-Ge heterostructure based on the use of 2D SnTe material has produced photovoltaic detector with high performance and minimal energy consumption.

2. Experimental

2.1 Preparation of SnTe/n-Ge heterostructure by a one-step magnetron sputtering method

SnTe/n-Ge heterostructure was prepared by a one-step magnetron sputtering. SnTe nanofilm was sputtered on to a pre-masked n-Ge substrate using a customized magnetron sputtering technique (SPS-T-S100N-2G, Weinaworld). Single SnTe target (99.99 % purity, purchased from Zhongnuo Advanced Material Technology) was used. Firstly, the n-type Ge (100) substrates (ρof 1-5 ohm·cm, single crystal, purchased from Rdmicro) was ultrasonic cleaned with acetone and then ethanol for 15 min, and blown dried using high-purity nitrogen. The n-Ge substrate was masked using aluminum (Al) foil and then placed in the vacuum chamber. SnTe nanofilm was deposited on to the pre-masked n-Ge substrate at a pressure of 7.5×10^{-4} pa using a low sputtering power of 80 W and at argon flow rate of 80 sccm without increasing the substrate temperature. After sputtering, the foil was removed and Al electrodes were deposited on to the SnTe nanofilm and Ge substrate by PVD.

2.2 Characterization of the structure, surface morphology and composition of as-prepared SnTe nanofilm

Transmission electron microscopy (TEM) characterization was conducted on a Tecnai G2 TF30 instrument. Atomic force microscope (AFM) images were obtained using Model Seiko SPA-400 instrument. Raman spectroscopy was

performed using a Renishaw inVia instrument at an excitation wavelength of 532 nm. Energy disperse spectroscopy (EDS) was performed using field-emission scanning electron microscope (SEM, Quanta 200) at 15 kV. X-ray photoelectron spectroscopy (XPS, K-Alpha+ instrument) was performed using AlKα radiation source having an energy of 1486.6 eV.

2.3 Characterization of SnTe/n-Ge heterostructure photovoltaic detector

Keithley 2400 digital source meter was used for *J-V* measurements on the SnTe/n-Ge heterojunction photovoltaic detector. Light emitting diodes (LEDs) having wavelength between 400 and 2050 nm were used as light source. Transient response measurement was carried out using the Keithley 2400 digital source meter with the LEDs actuated by function/arbitrary waveform generator (RIGOL, DG 1022U). All measurements were performed under ambient conditions at room temperature.

3. Results and discussion

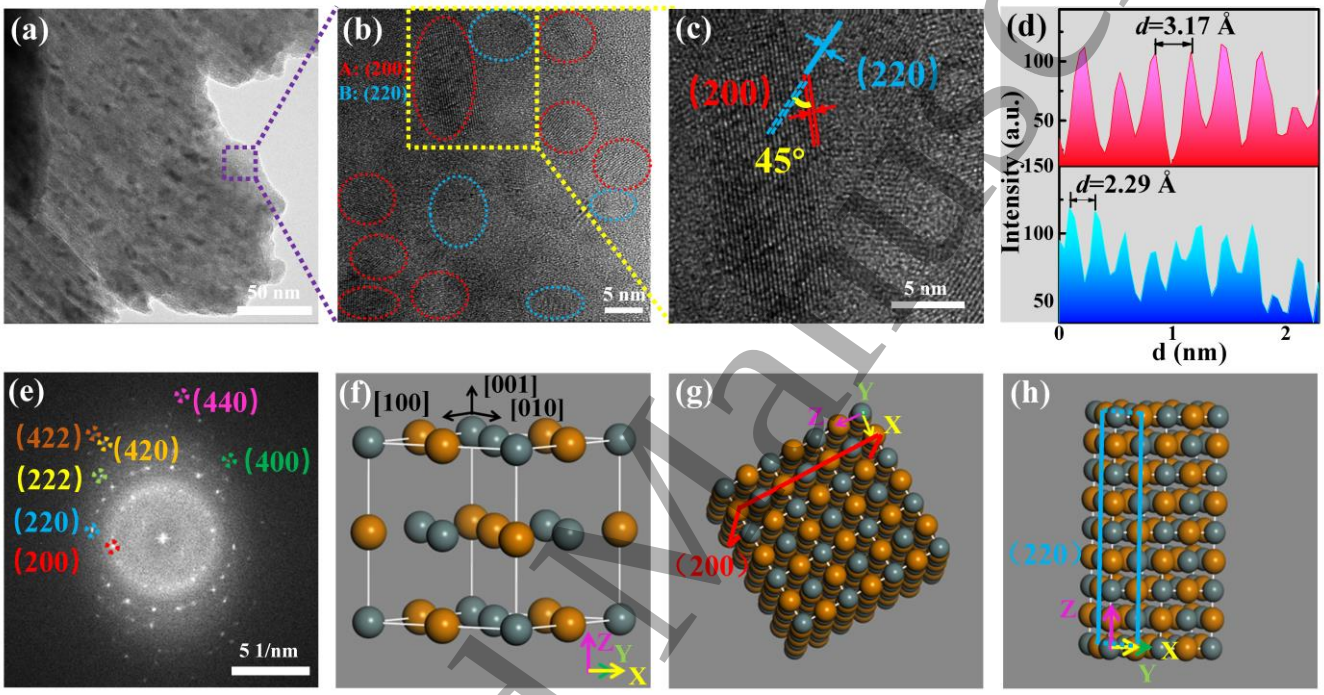

Figure 1. (a)-(c) TEM images of the as-prepared SnTe nanofilm. (d) Line profiles showing the interplanar spacings. (e) Fast Fourier transform (FFT) patterns of the SnTe nanofilm. (f)-(h) Schematic diagrams of SnTe crystal structures.

In order to study the crystal quality and structure of the as-prepared SnTe nanofilm, TEM characterization was carried out as shown in Figure 1(a)-(c). Figure 1(a) shows a low-resolution TEM image of the nanofilm. A high resolution TEM (HRTEM) image enlarged from a selected area in Figure 1(a) is shown in Figure (b). Multiple lattice fringes lattice fringes in the two directions, as shown in Figure (c), which further confirmed the two crystal planes and is consistent with the theoretical value. These clear lattice fringes in the HRTEM images indicated that the as-prepared nanofilm has a preferential growth direction at (200) and (220) crystal planes. Figure (d) shows the line profiles of the two lattice fringes. Figure 1(e) shows the fast Fourier transform (FFT) pattern obtained from the selected area of can be clearly seen in Figure 1(b). All lattice fringes were measured and compared with the cubic structure standard PDF card of SnTe (PDF#46-1210, Cubic, Fm3m (225)). It was found that the measured fringe spacings of 3.17 and 2.29 Å were consistent with the crystal planes (200) and (220), respectively. An angle of 45° was measured between the Figure 1(b). Based on the lattice fringe spacings (and according to the cubic SnTe standard PDF card) and the position of the bands formed by the apparent diffraction spots in Figure 1(e), the corresponding crystal planes of (200), (220), (222), (400), (420), (422) and (440) were marked on the transformation diagram. This indicated that the as-prepared SnTe nanofilm was polycrystalline and no other substance was found, which further suggested that the

nanofilm was of high quality face-centered cubic (FCC) crystal structure. The sputtered SnTe nanofilm was crystallized without increasing the substrate temperature and undergoing post-annealing treatment. Such simple and efficient preparation method is highly conducive in the production of low cost SnTe-based photodetector.

Figure 1(f) shows a schematic diagram of the FCC crystal structure of SnTe, where the yellow spheres represented Te atoms and the gray spheres represented Sn atoms. Schematic diagrams of (200) and (220) crystal planes are depicted in Figure 1(g) and (h), respectively. The presence of (200) and (220) crystal planes suggested that the as-prepared SnTe nanofilm has strong topological surface state characteristics [5].

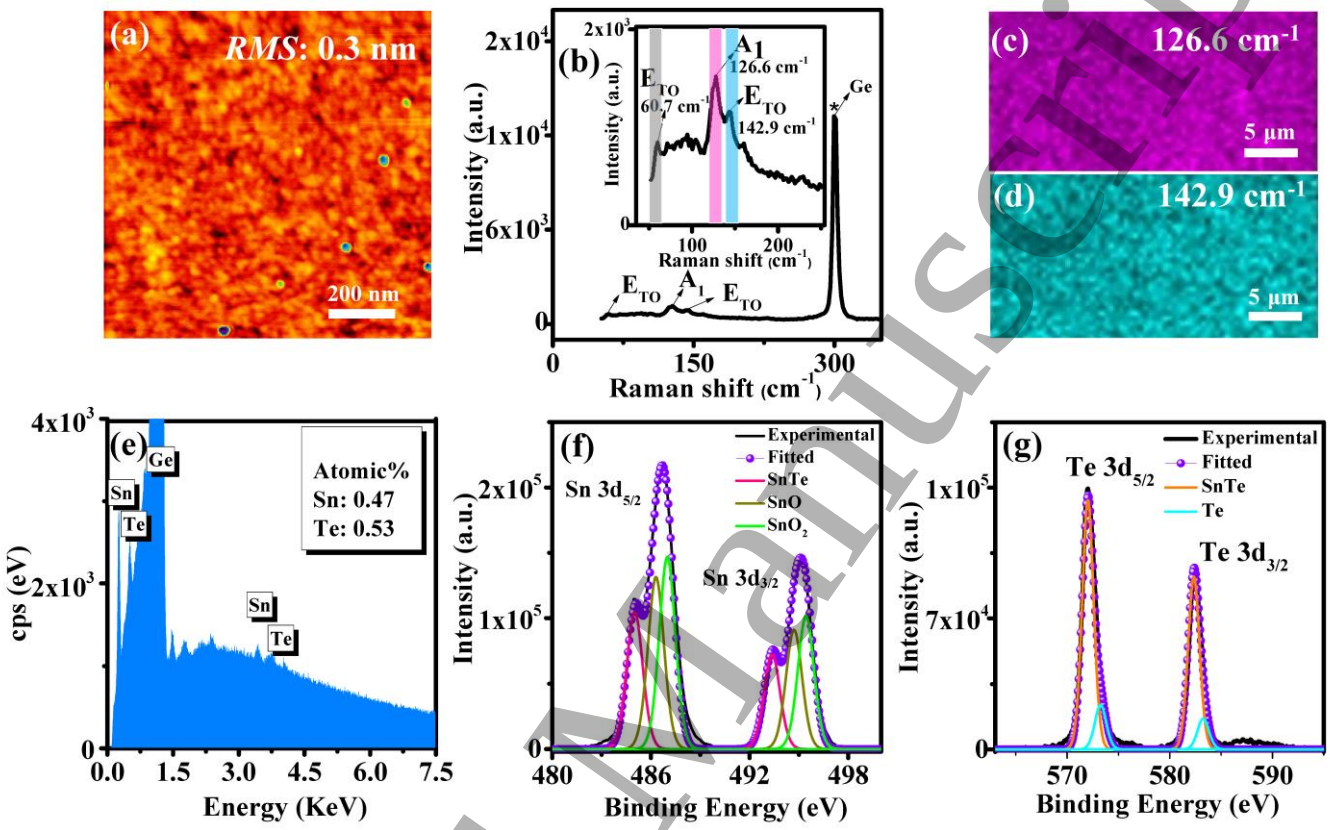

Figure 2. (a) AFM images of the as-prepared SnTe nanofilm. (b) Raman spectrum of the as-prepared SnTe nanofilm. (c) and (d) Raman mappings of peaks located at 126.6 and 142.9 cm^{-1}, respectively. (e) EDS spectrum of the as-prepared SnTe nanofilm. (f) and (g) XPS spectra of Sn 3d and Te 3d core levels of the as-prepared SnTe nanofilm, respectively.

Figure 2(a) shows an AFM image of the as-prepared SnTe nanofilm on Ge substrate. The as-prepared SnTe nanofilm exhibited uniform surface morphology at a scanned area of 200 nm × 200 nm. The particle size distribution of the nanofilm was relatively uniform with root mean square (*RMS*) surface roughness of 0.3 nm. Such small surface roughness was highly favorable in forming good metal contacts during device fabrication. Ramans pectroscopy was performed to further characterize the phase and crystal structure of the as-prepared SnTe nanofilm on Ge substrate as shown in Figure 2(b). Three peaks can be observed at 60.7, 126.6 and 142.9 cm^{-1}.The peak at 126.6 cm^{-1} corresponded to the transverse optical phonon mode (A_1), while the relatively weaker peaks at 60.7 and 142.9 cm^{-1} corresponded to phonon mode (E_{TO}). Compared with SnTe bulk material [12], the Raman peak at 142.9 cm^{-1} of the SnTe nanofilm was red-shifted by a few wave numbers, which may be attributed to the quantum size effect of the nanomaterials, similar to previously reported wok on SnS nanosized compounds [13], CdS quantum dots and BiI_3 nanocrystallites [14,15]. Raman mappings were performed for the peaks at 126.6 and 142.9 cm^{-1} as shown in Figure 2 (c) and (d), respectively, which further verified the high uniformity and good quality of the SnTe nanofilm.

EDS spectra of the SnTe nanofilm is shown in Figure 2(e). The results showed that the atomic ratio of Sn:Te was close to 1:1, which is consistent with the stoichiometric ratio of SnTe. This revealed that the as-prepared SnTe nanofilm has a precise chemical ratio [8]. The presence of Ge element in the EDS spectra was due to the Ge substrate.

XPS study was carried out to investigate the chemical bonding of elements in the as-prepared SnTe nanofilm on Ge substrate. Figure 2(f) and (g) show the XPS spectra of Te 3d

and Sn 3d core level peaks of the SnTe nanofilm, splitting peaks of Sn 3d core level were deconvoluted into three components representing Sn-Te bond (Sn $3d_{5/2}$ = 484.96 eV, Sn $3d_{3/2}$ = 493.36 eV), Sn^{2+}-O bond (Sn $3d_{5/2}$ =486.29 eV, Sn $3d_{3/2}$ = 494.76 eV) and Sn^{4+}-O bond (Sn $3d_{5/2}$ =486.92 eV, Sn $3d_{3/2}$ = 495.39 eV). The proportion of Sn-Te bond, Sn^{2+}-O bond and Sn^{4+}-O bond was 18.96, 23.9 and 26.69 %, respectively. Since there was an absence of Sn oxide in the TEM image, the observed oxides in the XPS spectra could be introduced during sample transfer and respectively. As shown in Figure 2(f), the spin-orbit measurements. The spin-orbit splitting peaks of Te 3d core level were deconvoluted into two components consisting of Sn-Te bond (Te $3d_{5/2}$ = 571.83 eV, Te $3d_{3/2}$ = 582.40 eV) and Te-Te bond (Te $3d_{5/2}$ = 573.51 eV, Te $3d_{3/2}$ =583.17 eV) as shown in Figure 2(g). The proportion of Sn-Te bond and Te-Te bond was 25.82 and 4.63 %, respectively. The appearance of Te-Te could be caused by Sn vacancies, which could lead to the neighboring Te atoms having non-bonding orbitals resulting in Te metallic state with higher binding energy [16].

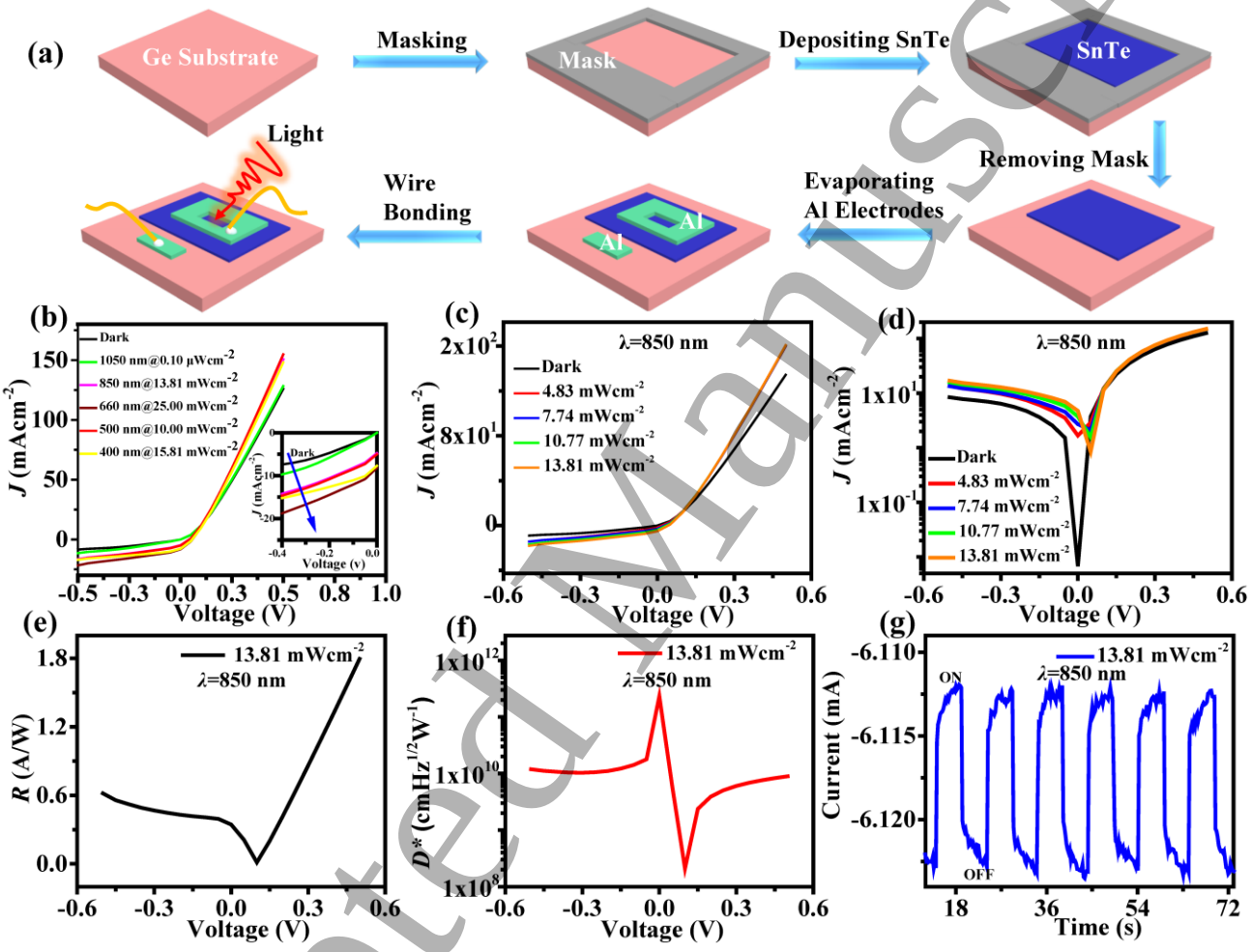

Figure 3. (a) Schematic diagrams illustrating the preparation process of SnTe/n-Ge photovoltaic detector. (b) *J-V* characteristics of the photodetector under dark (black line) and varying light illuminations (400-1050 nm). (c) and (d) *J-V* and log *J-V* plots of the photodetector under 850 nm illumination at bias voltage between -0.5 and 0.5 V, respectively. (e) and (f) Plots of responsivity (*R*) and detectivity (*D**) against *V* under the illumination of 850 nm at bias voltage between -0.5 and 0.5 V, respectively. (g) Photocurrent switching behavior of the photodetector at a voltage bias of -0.5 V under 850 nm illumination.

A prototype photovoltaic detector based on the as-prepared SnTe/n-Ge heterostructure was fabricated to explore its potential application in the field of photoelectric detection. The preparation process of the photodetector is shown in Figure 3(a). The thickness of the SnTe nanofilm was 5.8 nm (sputtering duration of 10 s). A quadrate window

with an area of 4 mm^2 was developed on the Al electrode to charge collection efficiency.

Figure 3(b) shows the *J-V* characteristic plots under dark condition and varying light illuminations (also an inset shows a magnified view of the characteristic at voltages between -0.4 and 0 V). As can be seen from the plots, the device demonstrated photoelectric response over a broadband between 400 and 1050 nm. The *J-V* and log *J-V* characteristics of the device under 850 nm near-infrared illumination and different power densities (*e.g.*, 4.83, 7.74, 10.77 and 13.81 mW/cm^2) are shown in Figure 3(c) and 3(d), respectively. An increase in the photocurrent density was observed with an increase in the incident light power density. Figure 3(d) shows that the as-prepared SnTe/n-Ge heterostructure exhibited good diode characteristics and the photocurrent density under 850 nm illumination was larger than the dark current density for negative bias voltage between -0.5 and 0 V. Similarly, the photocurrent density increased with an increase in the incident light power density under 850 nm illumination. The open circuit voltage of the photodetector was almost zero when the optical power density was relatively low at 4.83 mW/cm^2, and the open circuit voltage gradually increased with an increase in the optical power density. When the optical power density increased to 13.81 mW/cm^2, the open circuit voltage was 0.05 V. This showed that the photodetector was capable of working at small bias voltages, which is important to ensure stability of the device. Otherwise, high bias voltages could generate excess heat during device operation and therefore affecting device stability [17].

The responsivity (R) and detectivity (D^*) are two important parameters used to evaluate the performance of photodetector. Their calculations are shown in the following formulae.

$$R = J_p / P_{opt} \quad (1)$$

$$D^* = \frac{R}{\sqrt{2q|J_d|}} \quad (2)$$

where J_p is the photocurrent density, P_{opt} is the incident light power density, q is the unit charge, and J_d is the dark current density. The calculated results are plotted in Figure 3 (e) and (f) showing responsivity (R) and detectivity (D^*) against V, respectively, under the illumination of 850 nm at bias voltage between -0.5 and 0.5 V. SnTe was used as a p-type semiconductor material and therefore forming a p-n heterojunction with the n-Ge substrate. A strong built-in electric field was generated at the interface between the SnTe nanofilm and n-Ge substrate, which could effectively improve the separation and transmission of photocarriers. The R reached a value of 617.34 mA/W at -0.5 V, and the D^* reached a value of 2.33×10^{11} $cmHz^{1/2}W^{-1}$ at 0 V.

Table 1. Comparison of performances of heterostructure photodetectors based on based on SnTe/n-Ge, other 2D materials/Ge and SnTe/n-Si.

Materials	Wavelength (nm)	t_r (ms)	t_d (ms)	R (mA/W)	D^* (Jones)	Ref.
SnTe/n-Ge	400-2050	206 (850 nm)	267 (850 nm)	617 (850 nm)	2.33×10^{11} (850 nm)	This work
$PtSe_2$/Ge	1550	7.42×10^{-3}	16.71×10^{-3}	602	6.31×10^{11}	[18]
Graphene/Ge	1400	23×10^{-3}	108×10^{-3}	51.8	1.38×10^{10}	[19]
Ge/perovskite	405-1550	2.2	5.6	0.80×10^{3} (1550 nm)	9.1×10^{7} (1550 nm)	[20]
Graphene/Ge	1550	-	-	0.75×10^{3}	2.53×10^{9}	[21]
Titanium Nitride/Ge	2000	-	-	-	6.32×10^{5}	[22]
Graphene/Ge	1550	-	-	1.20×10^{3}	1.90×10^{10}	[23]
MoS_2/Ge	350-1100	-	-	16.3 (1000 nm)	-	[24]
SnTe/n-Si	254-1550	8×10^{-3}	0.39	128 (808 nm)	8.40×10^{12} (808 nm)	[10]
Commercial (Ge-	1550	10	10	950	2.50×10^{11}	

FDG10X10)

It is worth noting that the reported *R* value of the unoptimized photodetector was higher than that of previous work on SnTe/n-Si heterostructure, however the D^* value was lower than that of the heterostructure the SnTe/n-Si heterostructure[10]. The possible reasons for the high responsivity of the unoptimized photodetector are the use of a suitable preparation process for the SnTe film, which exhibited good uniformity and quality, hence allowing the formation of high quality SnTe/Ge heterostructure for photovoltaic application. This is important to enhance the separation and transmission efficiency of carriers that led to an improvement in the device performance. Photocurrent switching behavior of the photodetector at a voltage bias of -0.5 V under 850 nm illumination is shown in Figure 3(g). The rise time (t_r) and fall time (t_d) of the photodetector were 206 and 267 ms, respectively. The photoelectric performance of the photodetector remained stable after 3 months. Table 1 compares the performances of photodetectors consisting of heterostructures based on SnTe/n-Ge, other 2D materials/Ge and SnTe/n-Si as previously reported.

4. Conclusion

For the first time, a photovoltaic detector based on SnTe/n-Ge heterostructure was prepared by a one-step magnetron sputtering technique. The as-prepared SnTe/n-Ge heterostructure exhibited remarkable diode rectification characteristics at a small bias range of -0.5 to 0.5 V. It demonstrated photovoltaic characteristics in the broadband from visible light to near infrared (400-2050 nm). Under 850 nm near-infrared illumination, the responsivity (*R*) and detectivity (*D**) of the photodetector reached a value of 617.34 mA/W (at -0.5V bias) and 2.33×10^{11} $cmHz^{1/2}W^{-1}$ (at zero bias), respectively. A novel, low-cost, high performance and low power SnTe/n-Ge based broadband photovoltaic detector was developed in this work. The simple preparation of the SnTe nanofilm on n-Ge substrate using magnetron sputtering would provide an efficient method to study other novel 2D materials based photovoltaic detectors.

See Supplementary Materials for I-T characterization of the SnTe/n-Ge photodetector under1300, 1550, 1700 and 2050 nm LED light sources (Supplementary Figure S1).

Acknowledgments and funding

This work was supported by the National Key Research and Development Program (No. 2019YFB2203404), the National Natural Science Foundation of China (No. 61106098), the Program for Innovation Team of Yunnan Province (No. 2018HC020).

Data availability statement The data that support the findings of this study are available upon reasonable request from the authors.

References

[1] Tan G et al. 2015 *J. Am. Chem. Soc*. **137** 11507
[2] Liu J, Qian X F and Fu L, 2015 Nano Lett. **15** 2657
[3] Safdar M, Wang Q S, Mirza M, Wang Z X, Xu, K and He J 2013 Nano Lett. **13** 5344
[4] Taskin A A, Yang F, Sasaki S, Segawa K and Ando Y 2014 Phys. Rev. B **89** 991
[5] Hsieh T H, Lin H, Liu J W, Duan W H, Bansi A and Fu L 2012 Nature Commun. **3** 982
[6] Tanaka Y, Ren Z, Sato T, Nakayama K, Souma S, Takahashi T, Segawa K and Ando Y 2012 *Nat. Phys.* **8** 800
[7] Jiang T, Zang Y Y, Sun H H, Zheng X, Liu Y, Gong Y, Fang L, Cheng X A, and He K, 2017 *Adv. Opt. Mater*. **5** 1600727
[8] Liu J L, Li X, Wang H, Yuan G, Suvorova A, Gain S, Ren Y L, and Lei W 2020 *ACS Appl. Mater. Interfaces* **12** 31810
[9] Feng Y J, Chang H C, Liu Y B, Guo N, Liu J K, Xiao L, and Li L S 2021 *Nanotechnology* **32** 195602.
[10] Gu S H, Ding K, Pan J, Shao Z B, M J, Zhang X J and Jie J S 2017 *J. Mater. Chem. A* **5** 11171
[11] Zhang H B, Song Z L, Li D, Xu Y C, Li J, Bai C J and Man B Y 2020 *Appl. Surf. Sci.* **509** 145290
[12] Pal S et al. 2020 *Phys. Rev. B* **101** 155202
[13] Masoud S N, Mehdi B and Fatemeh D 2010 *Appl. Surf. Sci.* **257** 781
[14] Balandin A, Wang K L, Kouklin N and Bandyopadhyay S 2000 *Appl. Phys. Lett.* **76** 137
[15] Yang Y J, Wang C R, Hou J Q and Dai J M 2003 *Mater. Lett.* **57** 2185
[16] Haque A, Banik A, Varma R M, Sarkar I, Biswas K and Santra P K 2019 *J. Phys. Chem. C* **123** 10272
[17] Buscema M, Island J O, Groenendijk, D J, Blanter S I, Steele G A, Van d Z, Herre S J and Castellanos-Gomez A 2015 *Chem. Soc. Rev.* **44** 3691
[18] Wang L, Li J J, Fan Q, Huang Z F, Lu Y C, Wu C Y, Xie C and Luo L B 2019 *J. Mater. Chem. C* **7** 5019
[19] Zeng L H, *et al*. 2013 *ACS Appl. Mater. Interfaces* **5** 9362
[20] *Hu W, Cong H, Huang W, Huang Y, Chen L J, Pan A L, Xue C L* 2019 *Light-sci Appl.* **8** 10
[21] Kyoung, *et al*. 2019 *Adv. Electron. Mater.* **5** 1970028
[22] Shinde S L, Ishii S and Nagao T 2019 *ACS Appl. Mater. Interfaces* **11** 21965
[23] Kim C, Yoo T J, Chang K E，Min G K and Lee B H 2021 *Nanophotonics* **10** 1573
[24] Mahyavanshi R D, Golap K, Ajinkya R, Pradeep Desai, Masaharu K, Takehisa D, and Masaki T 2018 *IEEE Trans Electron Devices* **65** 443